Discrete FeII spin-crossover complexes of 2,2'-dipyridylamino- substituted s-triazine ligands with phenoxo, cyanophenoxo and dibenzylamino functionalities

Haley S. Scott, Tamsyn M. Ross, Wasinee Phonsri, Boujemaa Moubaraki, Guillaume Chastanet, Jean-Francois Létard, Stuart R. Batten, Keith S. Murray

Discrete Fe(II) spin crossover complexes of 2,2'-dipyridylamino-substituted s-triazine ligands with phenoxo, cyanophenoxo and dibenzylamino functionalities

Hayley S. Scott,[a] Tamsyn M. Ross,[a] Wasinee Phonsri,[a] Boujemaa Moubaraki,[a] Guillaume Chastanet,[b] Jean-François Létard,[b] Stuart. R. Batten,[a],[c] and Keith S. Murray*[a]

Abstract:

Four 2,2'-dipyridylamino-*s*-triazine-substituted ligands, each incorporating different aromatic substituents (phenoxo, 4-CN-phenoxo and benzylamino) with different degrees of bulk and flexibility have been formed and incorporated into a number of mononuclear Fe^{II} complexes of type *trans*-$[Fe^{II}(L)_2(NCX)_2]\cdot$Solv (where X = S, Se and BH_3). These ligands were designed to promote π-π stacking between complexes. The complexes reported have been comprehensively characterised using single crystal diffraction techniques in combination with magnetic susceptibility measurements. LIESST measurements have been performed on selected complexes. Light irradiation has shown the occurrence of a reversible photo-switching process at low temperature.

Introduction

Spin crossover (SCO)[1] is a process that can occur in d^4–d^7 transition metal complexes that are in the correct octahedral crystal field splitting state to allow a switching to occur between low spin (LS) and high spin (HS) states by application of temperature,[2] pressure[3] or light irradiation treatment.[4]In attempts to obtain highly cooperative SCO behaviour a diverse variety of ligands ranging from unidentate, bridging and chelating ligands, containing different donor atoms, have been incorporated into SCO systems in recent years.[1] The incorporation of 2,2'-dipyridylamino-1,3,5-triazine-based ligands, where coordination occurs via the chelating dipyridyl-groups, has been explored previously and the effect of placing different substituents onto a *s*-triazine-dipyridylamino moiety, each varying in size and flexibility has been investigated in relation to the resulting SCO behaviour of Fe^{II} derivatives.[5-7]

The ligands presented here incorporate a non-coordinating, aromatic substituent on to the triazine, in order to promote π-π stacking between complexes, an interaction which is known to promote cooperative SCO transitions.[8]

Ross *etal*.,[5] have contributed a significant portion of work in the field of monomeric *s*-triazine-dipyridylamino-based SCO complexes and this is particularly relevant to the present study since work on a number of these past examples has been continued and expanded upon here. Using the ligand DBB (N^2,N^2,N^4,N^4-tetrabenzyl-N^6,N^6-di-(pyridin-2-yl)-1,3,5-triazine-2,4,6-triamine) two polymorphs of formula α-*trans*-$[Fe^{II}(DBB)_2(NCS)_2]$, β-*trans*-$[Fe^{II}(DBB)_2(NCS)_2]$ and a third complex *trans*-$[Fe^{II}(DBB)_2(N(CN)_2)_2]\cdot 2CH_3CH_2OH$, have been reported.[5a] The two *trans*-$[Fe^{II}(DBB)_2(NCS)_2]$ polymorphs each revealed unique magnetic behaviour with α-$[Fe^{II}(DBB)_2(NCS)_2]$ displaying a relatively abrupt spin transition at $T_{1/2}$ ~170 K, and β-$[Fe^{II}(DBB)_2(NCS)_2]$ revealing a more gradual spin transition, at$T_{1/2}$ ~300 K. The compound *trans*-$[Fe^{II}(DBB)_2(N(CN)_2)_2]\cdot 2CH_3CH_2OH$, displayed a gradual one-step spin transition with $T_{1/2}$ ~280 K.

Further, important examples of monomeric Fe^{II} *s*-triazine-dipyridylamino-based complexes displaying SCO behaviour have been reported by Gamez *et al*.[6] More recently, Gamez *et al*.[6b] have reported a complex which we have also made in the current study, albeit as a different solvate. The complex, *trans*-$[Fe(DTT)_2(NCS)_2]\cdot 2CH_2Cl_2$ (where DTT = 4,6-diphenoxy-N,N-di-2-pyridyinyl-1,3,5-triazin-2-amine, (N.B. Gamez *et al*. label this ligand as L1) displays a very gradual transition centred at $T_{1/2}$ ~233 K, characterised by a Δ*T* 80 K (namely the temperature range within which 80% of the transition considered occurs) of 90 K. Thus, the polyfunctional *s*-triazine-dipyridylamino-based ligands discussed here have given an array of Fe^{II} SCO coordination complexes, which display a wide range of interesting magnetic properties, largely deriving from the intermolecular interactions afforded by the different substituents attached to the triazine, in combination with solvation affects within the crystalline forms.

The known ligands DBB,[5a]and DTT[6b] are reported here as well as two new ligands 4,4'-((6-(di(pyridine-2-yl)amino)-1,3,5-triazine-2,4-diyl)bis(oxy))dibenzonitrile, DBT, and 4-((4-chloro-6-(di(pyridin-2-yl)amino)-1,3,5-triazin-2-yl)oxy)benzonitrile, DBNT. We report here the structural and magnetic data for seven mononuclear Fe^{II} complexes of type $[Fe^{II}(L)_2(NCX)_2]\cdot$Solv (where X = S, Se or BH_3), incorporating these *s*-triazine-dipyridylamino-based ligands (Figure 1, Table 1).

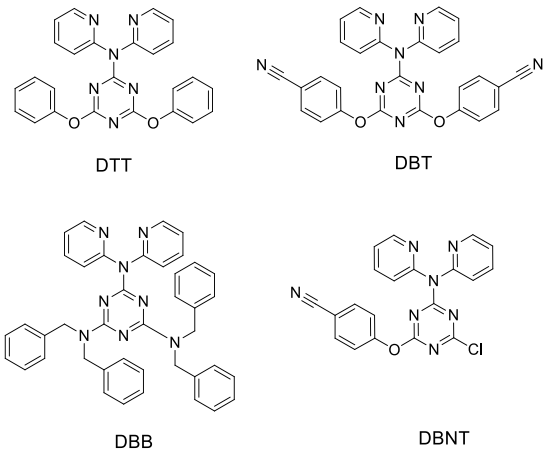

Figure 1. Molecular structure of *s*-triazine-dipyridylamino-based ligands used to form iron(II) complexes.

Results and Discussion

Syntheses and Characterisation

All complexes were synthesised by means of direct addition of a solution of $Fe^{II}(NCX)_2$ (in the relevant solvent) to a solution of two equivalents of the appropriate organic ligand. The resultant solution was then filtered and the filtrate left to either slowly evaporate (**1**-**4**, **7**) or sit in a sealed vial (**5**-**6**) for crystallisation to occur. Complexes **1**-**7** are listed in Table 1.

Table 1. Complexes formed and a summary of their magnetic behaviour. HS = high spin; SCO = spin crossover.

Compound		Magnetic behaviour	$T_{1/2}$(K)
trans-$[Fe^{II}(DTT)_2(NCS)_2]\cdot(H_2O)_{1/2}$	**1**	HS	-
trans- $[Fe^{II}(DTT)_2(NCSe)_2]\cdot(H_2O)_{1/2}$	**2**	HS	-
trans- $[Fe^{II}(DBT)_2(NCS)_2]\cdot 2MeOH$	**3**	Abrupt SCO	175
trans- $[Fe^{II}(DBT)_2(NCSe)_2]$	**4**	Abrupt SCO	280
trans- $[Fe^{II}(DBB)_2(NCSe)_2]\cdot 2MeCN$	**5a**	SCO (structural measurements)	-
trans- $[Fe^{II}(DBB)_2(NCSe)_2]$	**5b**	Incomplete broad SCO	-
trans- $[Fe^{II}(DBB)_2(NCSe)_2]\cdot 2MeCN$	**5c**	Incomplete abrupt SCO	330
trans- $[Fe^{II}(DBB)_2(NCBH_3)_2]\cdot 2MeCN$	**6**	Incomplete gradual SCO	360
trans- $[Fe^{II}(DBNT)_2(NCS)_2]\cdot 2MeOH$	**7**	Incomplete SCO	160

The complexes **5a**, **5b** and **5c** all co-crystallised in the same reaction vial. **5a** was only produced in very small quantities making bulk characterisation very difficult to achieve. As such, for **5a** the X-ray structure was determined at two temperatures, 123 K and 288 K (corresponding to the LS and HS states).

Complexes **5b** and **5c** formed in larger quantities and differences in colour and morphology of these crystals allowed them to be hand separated under a microscope; **5b** crystallises as yellow blocks while **5c** crystallises as thin red needles. Complexes **1**-**4**, **5c**, **6** and **7** all produced very small crystals. All of these complexes required synchrotron radiation for crystallographic structural determination to be carried out.

The two monomeric complexes $[Fe^{II}(DTT)_2(NCS)_2]\cdot(H_2O)_{1/2}$ (**1**) and $[Fe^{II}(DTT)_2(NCSe)_2]\cdot(H_2O)_{1/2}$ (**2**) have been synthesised and the structures of solvates of **1** and **2**, $[Fe^{II}(DTT)_2(NCX)_2]\cdot 5.5CHCl_3$ (where X = S and Se), have been previously reported but without further characterisation.[5d] Furthermore, and as previously mentioned, Gamez *et al*., have reported additional solvates to **1** and **2**, $[Fe(DTT)_2(NCS)_2]\cdot 2CH_2Cl_2$ and $[Fe(DTT)_2(NCSe)_2]\cdot 4CH_2Cl_2\cdot 4CH_3OH$ each of which showed gradual SCO with $T_{1/2}$ occurring at ~233 and ~238 K, respectively.[6b] A comparative discussion between the two sets of complexes is given later.

Octahedral distortion parameters Σ[9] and Θ[10] have been calculated for all complexes and these appear in Table S2.

Structural Descriptions

Crystal structures of complexes 1 and 2

Complexes **1** and **2** are isostructural, crystallising in the tetragonal space group $P4_2/n$, and their structural data were determined at 100 K. The central Fe^{II} is coordinated by two bidentate DTT ligands bound via the N-donors of the 2,2'-dipyridylamino group. The FeN_6 donor set is completed by two anionic cyano-based *trans*-oriented NCX$^-$ ligands binding through the N-atom (Figure 2). At 100 K, the Fe-$N_{(NCX)}$ and average Fe-$N_{(DTT)}$ bond lengths are equal to 2.086(2)Å and 2.246(2) Å, respectively, for complex **1**, and 2.069(3) and 2.221(3) Å, respectively, for complex **2**. These values suggest the Fe^{II} centre of each complex occupies the HS state at this temperature. Other pertinent bond lengths and angles for complex **1**–**7** are given in Tables S1 and S2.

There is a single H_2O molecule in the outer coordination sphere of complexes **1** and **2**. The O-atom of the water (O3) is disordered across (**1**), or sitting on (**2**), a site of -4 symmetry. Hydrogen atoms are therefore disordered and have not been placed on the solvent molecule. The orientation of the phenoxy rings can be best described as resembling a "T" shape, where they extend out and are oriented approximately 90º to the triazine ring (Figure 2). π-π stacking exists between mononuclear complexes via the centroid of a coordinating pyridyl ring and C18, which is located on a phenoxy group, centroid…C18 = 3.45 Å for complex **1** and 3.47 Å for complex **2**. This interaction results in an overall 1D structure (Figure S1, top). The O3 atom also H-bonds to the N7 of four surrounding triazine rings with the O3...N7 distance equal to 3.368(2) Å for **1** and 3.374(2) Å for **2**. There are additional intermolecular CH…π interactions occurring between 1D chains with a centroid…H25(C25) distance equal to 2.76 Å for **1** and 2.71 Å for **2** (Figure S1, bottom).

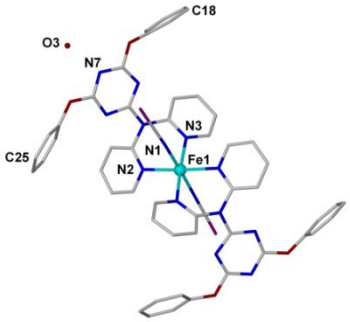

Figure 2. Structure of complex **1** (isostructural to **2**). H atoms omitted for clarity.

Complexes 3 and 4

Complex **3** crystallises in the orthorhombic space group $Pca2_1$ and its structure was determined at 100 K. The central Fe^{II} is coordinated by two bidentate DBT ligands bound via the N-donors of the 2,2'-dipyridylamino group. The FeN_6 donor set is completed by two anionic cyano-based *trans*-NCX$^-$ ligands binding through the N-atom (Figure 3). The average Fe-$N_{(NCS)}$ and Fe-$N_{(DBT)}$ bond lengths are equal to 1.980(2) Å and 2.018(3) Å, respectively, indicating the Fe^{II} occupies the LS state at this temperature. The *cis* and *trans* N-Fe-N angles range between 85.65(11)–94.04(11)º and 179.39(10)–179.85(12)º, respectively. The rings of the benzonitrile moiety are orientated in an "L" shape, with one pointing "up" from the centre of the complex, and the second pointing "sideways". There are two MeOH solvent molecules in the outer coordination sphere. Each MeOH hydrogen bonds to separate N-triazine groups. {N14…H50(O5) 2.019(3) Å and N9...H60(O6) 2.123(3) Å} (Figure 3).There are further, weaker hydrogen bonds between a terminal nitrile and pyridyl hydrogens of two adjacent complexes (N11…H27(C27) 2.572(2) Å, N11…H24(C24) 2.591(3) Å, Figure S2). These weak interactions connect the complexes into layers in the *xz* plane. Each complex connects to four others - two via its nitrile N11 nitrogen, and two via the H24 and H27 protons (which are on opposite sides of the same pyridyl ring), to give a corrugated sheet with (4,4) topology.

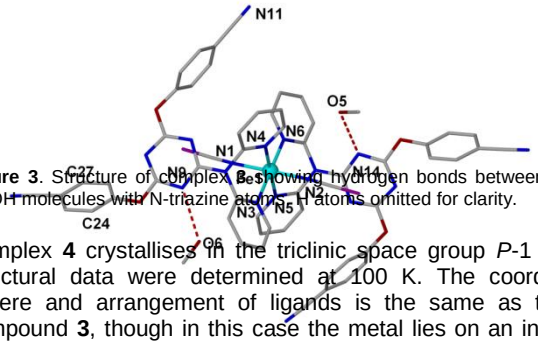

Figure 3. Structure of complex **3** showing hydrogen bonds between solvent MeOH molecules with N-triazine atoms. H atoms omitted for clarity.

Complex **4** crystallises in the triclinic space group *P*-1 and its structural data were determined at 100 K. The coordination sphere and arrangement of ligands is the same as that for compound **3**, though in this case the metal lies on an inversion centre rather than on a general position. The average Fe-$N_{(NCSe)}$ and Fe-$N_{(DBT)}$ bond lengths are equal to 1.9427(17) Å and 1.9849(14) Å respectively, indicating the Fe^{II} ion occupies the LS state at this temperature. The *cis* N-Fe-N angles range between 87.01(6)–92.99(6)º. Unlike **3**, complex **4** has no solvent molecules in the outer coordination sphere. The orientation of the benzonitrile groups in **4** differ from **3** in that both are directed "up" from the complex and therefore adopt a "Y" conformation (Figure 4).

Similar to complex **3**, weak hydrogen bonding exists between nitriles and aromatic hydrogen atoms. In **4**, however, every nitrile of the complex is involved in hydrogen bonding (N9…H9(C9) 2.542(4) Å, N8…H23(C23) 2.550(4) Å) with each complex making eight hydrogen bonds to four adjacent complexes (connecting to each complex once via a nitrile nitrogen and once via an aromatic hydrogen). This gives, overall, a planar (4,4) sheet motif. Because the structural data were collected at a temperature in the LS state, upon transition to the HS state (with elongation of Fe-N bond lengths) this may lead to a further shortening of these interactions.

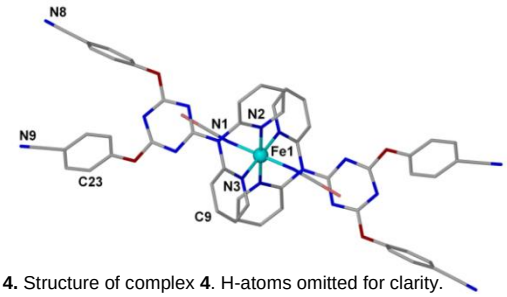

Figure 4. Structure of complex **4**. H-atoms omitted for clarity.

Complexes 5a, 5b, 5c and 6

Previous complexes incorporating the DBB ligand include α-$[Fe^{II}(DBB)_2(NCS)_2]$, β-$[Fe^{II}(DBB)_2(NCS)_2]$ and $[Fe^{II}(DBB)_2(N(CN)_2)_2]\cdot 2EtOH$.[5a] Because the abovementioned complexes all show SCO behaviour, we pursue here the formation of complexes binding stronger ligand-field anionic NCX$^-$ ligands *viz.* $[Fe^{II}(DBB)_2(NCSe)_2]$ (**5**) and $[Fe^{II}(DBB)_2(NCBH_3)_2]$ (**6**).

The crystal structures of three different crystalline products of complex **5** were solved. **5a** formed as yellow block-shaped crystals and data were collected at two different temperatures 123 K and 288 K, corresponding to the LS and HS states. Full structural determinations of complexes **5b** and **5c** were only made at one temperature, *viz.* 123 and 100 K, respectively.

Complex 5a

Complex **5a** crystallises in the triclinic space group *P*-1 and data were collected at both 123 K and 288 K. The central Fe^{II} ion lies on an inversion centre and is coordinated by two bidentate DBB ligands bound via the N-donors of the 2,2'-dipyridylamino group. The FeN_6 donor set is completed by two anionic cyano-based *trans*-NCX$^-$ ligands binding through the N-atom. At 123 K the average Fe-$N_{(NCSe)}$ and Fe-$N_{(DBB)}$ lengths are 1.964(1) Å and 2.038(2) Å, respectively, indicating the Fe^{II} occupies the LS state at this temperature. The *cis* N-Fe-N angles range between 85.19(7)–94.81(7)º. The octahedral distortion parameter Σ is equal to 26°, the Θ value was calculated to be 43º. There are two MeCN in the outer coordination sphere. Closest intermolecular contacts exist between MeCN solvent molecules and H-atoms of the pyridyl rings. (N10…H4(C4) 2.916(3) Å, N10…H5(C5) 2.814(2) Å, N10…H8(C8) 2.932(2) Å) (Figure 5). Closest contact interactions for **5a** are listed in Table 2. These include off-set π-π interactions occur between phenyl groups of benzyl arms yielding 1D motifs (ESI, Fig. S5).

Data collection for **5a** was also made at 288 K and this again indicated the triclinic space group *P*-1 for the crystal. The average Fe-$N_{(NCSe)}$ and Fe-$N_{(DBB)}$ lengths at this temperature correspond to 2.082(2) Å and 2.231(2) Å, respectively, indicating the Fe^{II} occupies the HS state. The *cis* N-Fe-N angles range between 81.63(7) – 98.37(7)°. The octahedral distortion parameter Σ is equal to 46° and the Θ value was calculated to be 74º. There are two MeCN in the outer coordination sphere. Hydrogen bonding exists between MeCN solvent molecules and H-atoms of the dpa-pyridyl rings. Closest intermolecular contacts occur between MeCN solvent molecules and H-atoms of the pyridyl rings (N10…H4(C4) 2.990(2) Å, N10…H5(C5) 2.863(4) Å, N10…H8(C8) 2.889(4) Å). While the distance between the N10…H4(C4) and N10…H5(C5) contacts increases with temperature, interestingly the N10…H8(C8) distance decreases at higher temperature, suggesting a stronger interaction occurs in the latter.

In accordance with previous studies,[9,10] parameters Σ and Θ become smaller as the spin transition takes place for **5a**, as the distortion of the first coordination sphere is reduced going to the LS form (Table S2). This feature is further explored in the discussion section.

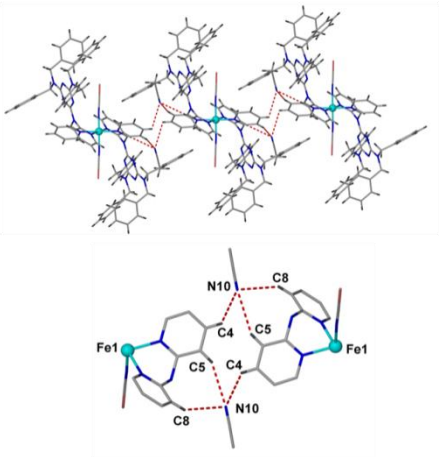

Figure 5. (Top). Closest intermolecular contacts in **5a** shown by red dotted lines. (Bottom). Close-up of the intermolecular contacts between solvent and pyridyl-H-atoms. Only hydrogen atoms participating in hydrogen bonding have been shown.

As previously mentioned, **5a** only formed in very small quantities ruling out the possibility of further characterisation, and so these two crystallographic results give us an indication of the spin transition for this complex, which appears to occur between 123 – 288 K.

Complex 5b

Complex **5b** crystallises in the monoclinic space group $P2_1/n$ and data were determined at 123 K with one half of the complex completing the asymmetric unit. The ligand binding modes and coordination sphere are the same as those described for **5a**. The Fe-$N_{(NCSe)}$ andFe-$N_{(DBB)}$ bond lengths are equal to 1.935(1) Å and 1.980(2) Å, respectively, indicative of the Fe^{II} sites occupying the LS state at 123 K. The *cis* N-Fe-N angles range between 86.34(6) – 93.66(6)°. There are no solvent molecules in the outer coordination sphere. Intramolecular X…πinteractions occur between the axial $NCSe^-$ ligands and the central *s*-triazine 'core' of DBB ligands (Se…$centroid_{triazine}$ 3.51 (Å)). There is also a number of close CH…π interactions between adjacent complexes. The packing diagrams of these are shown in Figure S5 and details listed in Table 2.

Complex 5c

Complex **5c** crystallises in the triclinic space group *P*-1 and its structural data were determined at 100 K. The binding modes of the ligands are the same as those for **5a** and **5b**. Similar to polymorph **5a**, there are two MeCN solvent molecules in the outer coordination sphere. The Fe-$N_{(NCSe)}$ and Fe-$N_{(DBB)}$ bond lengths are equal to 1.938(4) Å and 1.984(4) Å, respectively, indicating the Fe^{II} occupies the LS state at this temperature. The *cis* N-Fe-N angles range between 86.89(16) - 93.11(16)°. Two of the aromatic rings of the DBB ligand are disordered in this structure. In the first ring, three atoms (C34, C35 and C36) have been modelled over two positions each with 50% occupancy (Figure 6). The entire benzyl group, including the CH_2 arm, is disordered over two positions in the second ring and these have again been assigned to 50% occupancy. There are a number of close C..C interactions between molecules, these are shown in Figure S6 and they are listed Table 2. A structural comparison between complexes **5a, 5b** and **5c** is given in Figure 7.

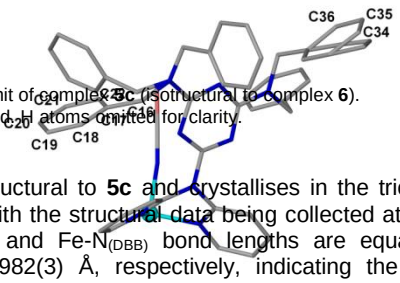

Figure 6. Asymmetric unit of complex **5c** (isotructural to complex **6**). Disordered atoms labeled, H atoms omitted for clarity.

Complex 6

Complex **6** is isostructural to **5c** and crystallises in the triclinic space group *P*-1, with the structural data being collected at 100 K. The Fe-$N_{(NCBH3)}$ and Fe-$N_{(DBB)}$ bond lengths are equal to 1.963(3) Å and 1.982(3) Å, respectively, indicating the Fe^{II} occupies the LS state at this temperature. The *cis* N-Fe-N angles range between 86.89(12) - 93.11(12)°. Because **5c** and **6** are isostructural, the disorder modelled for **5c** is the same in complex **6**.

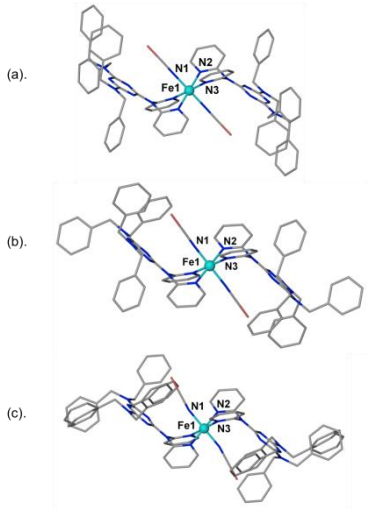

Figure 7. Monomeric complexes in (a) **5a**, (b) **5b**, (c), **5c** (isostructural to **6**).

Table 2. Closest interactions within complexes **1**-**7**.

Complex	Type of contact	Closest contacts	DH…A (Å)
1	π…π	$centroid_{pyridyl}$...C18	3.45
1	H-bond	O3...N7	3.368(2)
1	CH...π	$Centroid_{phenoxy}$...(H25)C25	2.76
2	π…π	$centroid_{pyridyl}$...C18	3.47
2	H-bond	O3...N7	3.374(2)
2	CH...π	$centroid_{phenoxy}$...(H25)C25	2.71
3	H-bonds	N14...(H50)O5	2.019(3)
3	H-bonds	N9...(H60)O6	2.123(3)
3	H-bonds	N11...(H27)C27	2.572(2)
3	H-bonds	N11...(H24)C24	2.591(3)
4	H-bonds	N9...(H9)C9	2.542(4)
4	H-bonds	N8...(H23)C23	2.550(4)
5a (123 K)	π…π	$Plane_{phenyl}$…$Plane_{phenyl}$	3.44
5a (123 K)	π…π	$Plane_{phenyl}$…$Plane_{phenyl}$	3.36
5a (123 K)	H-bond	N10…(H4)C4	2.916(3)
5a (123 K)	H-bond	N10…(H5)C5	2.814(2)
5a (123 K)	H-bond	N10…(H8)C8	2.932(2)
5a (288 K)	π…π	$Plane_{phenyl}$…$Plane_{phenyl}$	3.45
5a (288 K)	π…π	$Plane_{phenyl}$…$Plane_{phenyl}$	3.32
5a (288 K)	H-bond	N10…(H4)C4	2.990(2)
5a (288 K)	H-bond	N10…(H5)C5	2.863(4)
5a (288 K)	H-bond	N10…(H8)C8	2.889(4)
5b	π...CH	$centroid_{triazine}$...(H33)C33	3.307
5b	π...CH	$centroid_{phenyl}$...(H3)C3	2.593
5b	π...CH	$centroid_{phenyl}$...(H36B)C36	2.889
5b	π...CH	$centroid_{phenyl}$...(H39)C39	3.177
5c and **6**	C...CH	C10...(H3)C3	3.239(7)
5c and **6**	C...CH	C32...(H25)C25	2.774(7)
5c and **6**	C...CH	C43...(H28)C28	3.058(7)
7	H-bond	N17…(H2A)O2	2.182(2)
7	π…π	$centroid_{pyridyl}$…$centroid_{pyridyl}$	3.55

Complex 7

Complex **7** crystallises in the triclinic space group *P*-1 and its structural data were collected at 100 K. The central Fe^{II} is coordinated by two bidentate DTBN ligands bound via the N-donors of the 2,2'-dipyridylamino group. The FeN_6 donor set is completed by two anionic cyano-based *trans*-NCS$^-$ ligands binding through the N-atom (Figure 8). The *cis* N-Fe-N angles range between 83.02(7)-96.98(7)° and the average Fe-$N_{(NCS)}$ and Fe-$N_{(DBTN)}$ bond lengths are equal to 2.096(2) Å and 2.214(2) Å, respectively, indicating that the Fe^{II} occupies the HS state at 100 K. There are two MeOH solvent molecules in the outer coordination sphere and these were found to be hydrogen bonded to a nitrogen of the triazine ring, N17...H2A(O2), 2.182(2) Å. There is also additional π-π stacking between pyridyl

rings of adjacent monomers with centroid...centroid distances equal to 3.55 Å (Figure S7)

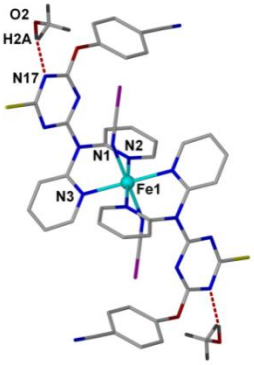

Figure 8. S

Magnetic

The vari
complexe
remains l
of 3.8 c
following
decrease due to zero-field splitting effects.

For complex **2** (Figure 9(a)) the $\chi_M T$ value of 3.50 cm^3 K mol^{-1} at 300 K remains essentially constant until around 220 K below which it slightly increases to a value of 3.60 cm^3 K mol^{-1} at 40 K. Further cooling beyond 40 K leads to the $\chi_M T$ value decreasing to reach a final $\chi_M T$ value of 3.00 cm^3 K mol^{-1} at 5 K, due, as in **1**, to zero field splitting effects. The origin of the slight increase in $\chi_M T$ between the temperature range 300–40 K, noted for **2**, which is also HS, is probably due to differences in orbital contribution and ligand-field asymmetry compared to **1**.

Complex **3** (Figure 9(b)) is shown to undergo a relatively abrupt spin transition, with $T_{1/2}$ occurring at ~175 K. A $\chi_M T$ value of 3.5 cm^3 mol^{-1} K observed at 300 K gradually decreases following cooling down to 200 K, where the $\chi_M T$ value is equal to 3.0 cm^3 mol^{-1} K. Further cooling yields a more abrupt decrease in $\chi_M T$ down to 100 K where a $\chi_M T$ of 0.20 cm^3 mol^{-1} K is measured, this value remains constant with further cooling down to 2 K. Hysteretic behaviour was not observed during the heating and cooling modes.

Complex **4** (Figure 9(b)) was found to undergo an abrupt spin crossover between the temperature range 2 – 350 K. At 350 K and following the cooling mode, an initial $\chi_M T$ value of 3.6 cm^3 mol^{-1} K decreases gradually down to 3.3 cm^3 mol^{-1} K at 300 K. Further cooling yields an abrupt decrease in $\chi_M T$ to 0.7 cm^3 mol^{-1} K at 255 K. Cooling to 2 K gives a gradual reduction in $\chi_M T$ to a final value of 0.2 cm^3 mol^{-1} K. A small hysteresis gap of 3 K was observed in the heating and cooling modes which is surprising in view of the weak H-bonding intermolecular contacts. $T_{1/2\uparrow}$ occurs at 281 K and $T_{1/2\downarrow}$ at 278 K.

Susceptibility measurements were not able to be performed on complex **5a** due to insufficient sample. The variable temperature magnetic susceptibility data for complexes **5b** and **5c** are shown in (Figure 9(c)). Complex **5b** showed a gradual and incomplete SCO over the temperature range 5–350 K. At 350 K a $\chi_M T$ value of 2.25 cm^3 mol^{-1} K was indicative of a spin crossover and this value gradually decreases, in a somewhat atypical manner, perhaps due to HS trapping, during cooling, to reach 0.17 cm^3 mol^{-1} K at 5 K, the sample being largely in the LS state. Interestingly, the structure at 100 K showed a LS structure.

For complex **5c**, an abrupt but incomplete spin transition was observed with $T_{1/2}$ ~ 320 K. At 350 K a $\chi_M T$ value of 2.19 cm^3 mol^{-1} K began to decrease rapidly with cooling to 275 K where $\chi_M T$ reached 0.17 cm^3 mol^{-1} K. Further cooling below this point showed a LS plateau in the $\chi_M T$ values of 0.02 cm^3 mol^{-1} K, in agreement with the LS nature of the crystal structure.

Complex **6** (Figure 9(d)) undergoes a gradual spin transition
ating from 130 K (not shown); plot 1. At 400 K, a $\chi_M T$
3.1 cm^3 mol^{-1} K is still not at the HS plateau value. It
es gradually upon cooling (plot 2), reaching 0.6 cm^3 mol
25 K. Further cooling beyond this temperature shows an
ore gradual reduction in $\chi_M T$ to reach 0.4 cm^3 mol^{-1} K at
dicative of the LS state. A second cycle, after heating in
UID chamber, follows the same trend in magnetic
bility, but with higher $\chi_M T$ values below 350 K
ing a loss of MeCN solvent occurs above 350 K.

7 shows a gradual incomplete crossover over the
ture range 6–350 K (Figure 9(e)). From 350–200 K only
gradual reduction in $\chi_M T$ from 3.1–2.8 cm^3 mol^{-1} K is
d. Further cooling to 150 K reveals a more abrupt
e in $\chi_M T$ to 2.4 cm^3 mol^{-1} K. Cooling from 150–6 K again
a gradual reduction in $\chi_M T$ to reach a plateau value of
^{3} mol^{-1} K down to ~40 K, then a rapid decrease due to
-field splitting, to reach a final value of 1.78 cm^3 mol^{-1} K
The data suggest either a spin transition occurs at $T_{1/2}$
but HS trapping prevents LS values being achieved, or it
tial spin crossover example in which HS and LS forms
The crystal structure at 100 K is indicative of the HS
dominating. Further structures at different temperatures
anted here.

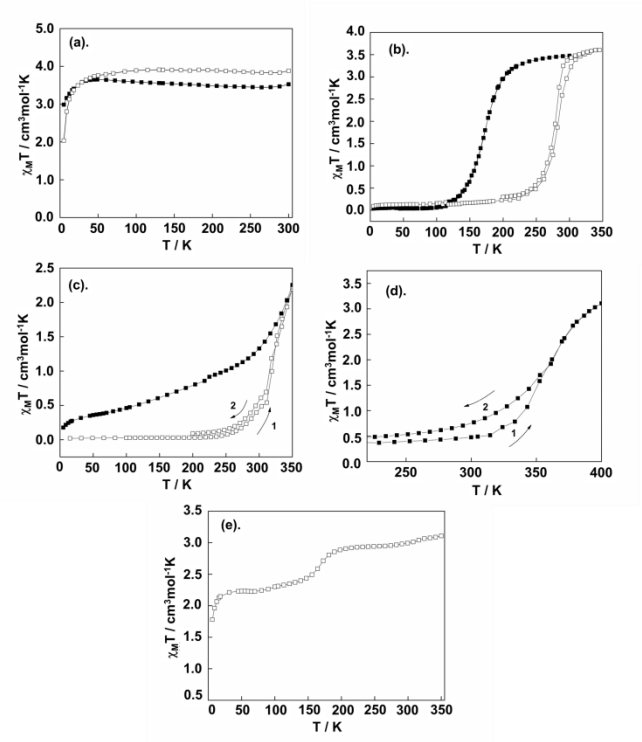

Figure 9. Variable temperature magnetic susceptibility ($\chi_M T$) measurements for complexes **1** - **7**. (a) **1**(□) and **2**(■); (b) **3**(■) and **4**(□); (c) **5b**(■) and **5c**(□); (d) **6**(■); (e) **7**(□).

Photomagnetic LIESST Studies on Complex 3

Complexes **3** and **4** were explored for any LIESST behaviour and only complex **3** shows an efficient photoswitching. Irradiation was tested at different wavelengths and the best one was found to be in the green region (532 nm) when employing a 5mW/cm^2 power laser. Almost all the molecules are converted from their LS states to the HS state (Figures 10 and 11). After irradiation, a relaxation in the dark was recorded during one hour to evaluate the stability of the HS photo-induced state (Figure 10). A slight decrease of the HS fraction occurs during this hour. To check the occurrence of the reverse-LIESST process, a new

irradiation at 532 nm was performed and followed by irradiation at 830 nm. A decrease of the HS fraction is observed which is of greater magnitude than the decrease in the dark. Therefore, the decrease observed under irradiation at 830 nm is due to a reverse-LIESST effect indicating the reversibility of the photo-induced process.

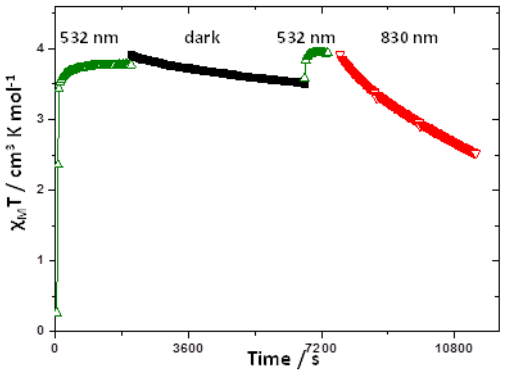

Figure 10. . Evolution of the $\chi_M T$ product of **3** at 10 K under 532 nm irradiation (Δ), 830 nm (Δ) and in the dark (●) after photo-excitation at 532 nm

After the irradiation at 532 nm, the *T*(LIESST) curve was recorded (Figure 11).[11,12] The increase of $\chi_M T$ from 10 to 25 K usually follows from the HS iron(II) zero-field splitting. The maximum $\chi_M T$ value is, rather surprisingly, higher at 25 K than at 250 K. This could follow from some orientation effects occurring under the 2 T magnetic field applied due to the large zero-field splitting of the complexes as already reported on the $[Fe(ptz)_6](BF_4)_2$ compound.[13] Above 25 K the $\chi_M T$ product rapidly decreases and the baseline is recovered. The minimum value of the derivative $\delta\chi_M T/\delta T$ gives the position of the *T*(LIESST) temperature estimated at 42 K. Let us note that the derivative $\delta\chi_M T/\delta T$ curve exhibits two close minima indicating a two-step *T*(LIESST) curve. This is quite surprising since no clear evidence of steps in the thermal spin-crossover curve was noticed. This could arise from the presence of short and long range interactions in the systems or the presence of two distinct iron(II) sites in the HS photo-induced state.

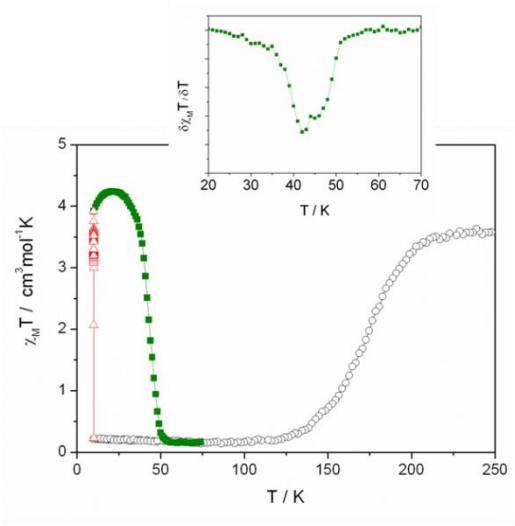

Figure 11. Thermal behaviour of the $\chi_M T$ product of **3** before irradiation (o), during irradiation (Δ) and in the dark after irradiation (■). The insert presents the derivative of the thermal behaviour in the dark after irradiation whose minimum allows the determination of the *T*(LIESST) value.

Several kinetics plots have been recorded to characterise the relaxation process (Figure 12). The relaxation curves are very slightly sigmoidal, but present also a stretched shape. This agrees with the two steps observed in the *T*(LIESST) curve. Both relaxation processes occur simultaneously and without a clear knowledge of the relative proportions of both processes simulations become very difficult with many parameters. To have a rough idea of the relaxation rate constant at each temperature, we have considered a stretched exponential law.[11] Figure 12 reports the fit of the kinetics obtained with this approach. Using the Arrhenius plot (ln k_{HL} *vs.* 1/T, insert Figure 12) the following thermodynamic parameters were found: E_a = 165 cm^{-1}; k_∞ = 0.25 s^{-1}; σ = 10 cm^{-1}. Obviously models including two relaxation processes could improve the fitting procedure but it is beyond the scope of this article to go into such details.

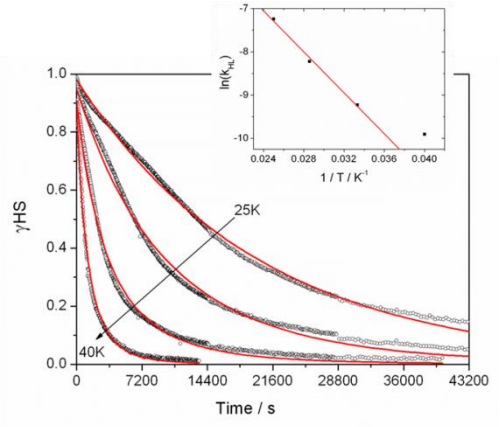

Figure 12. Plot of the different relaxation kinetics recorded as a function of the temperature for **3**. The red lines are the fits discussed in the text. The insert presents the Arrhenius plot.

Discussion

Seven mononuclear Fe(II) complexes of type $FeL_2(NCX)_2$ have been described, where L is a substituted dipyridylamino-triazine bidentate ligand (Figure 1), all exhibiting NCX^- anions in the *trans* configuration, with most of the compounds displaying SCO. The DTT complexes **1** and **2**, however, are HS at all temperatures thus indicating that even the combination of DTT and NCSe does not produce a ligand field strong enough to yield SCO. This contrasts with the gradual SCO noted by Gamez *et al.* for the related complexes $[Fe(DTT)_2(NCS)_2]\cdot 2CH_2Cl_2$ and $[Fe(DTT)_2(NCSe)_2]\cdot 4CH_2Cl_2\cdot 4CH_3OH$.[6b] Possible reasons why **1** and **2** remain HS in comparison to Gamez' complexes must include the nature of the solvation since the coordinated groups are the same in the NCS and NCSe pairs. The structural differences involving the solvate molecules are discussed further, below, under "solvent effects".

The DBT complexes **3** and **4** both show abrupt SCO, the latter with a small thermal hysteresis. Both, therefore, display cooperativity. Possible reasons for cooperativity are likely to result from the intermolecular interactions between complexes in both **3** and **4** which were discussed in the structure descriptions.

The pseudo-polymorphs **5b** and **5c** show notable differences in SCO behaviour with **5b** showing a very broad SCO and **5c** exhibiting an abrupt, but incomplete SCO, with $T_{1/2}$~330 K. Each of these complexes displays a number of different CH…π and CH…C interactions (closest contacts listed in Table 2). This exemplifies the importance that the effect of packing has on the overall magnetic properties of a complex.

DBB complexes **5a** and **5c** are polymorphs and each contains two acetonitrile solvent molecules in their outer coordination spheres. While they both crystallise in the triclinic space group *P*-1 their unit cell parameters reveal them to be crystallographically distinct. This is similar to the observed polymorphism for the analogous and previously reported compounds α-$[Fe^{II}(DBB)_2(NCS)_2]$ and β-$[Fe^{II}(DBB)_2(NCS)_2]$[5a] in

which it was suggested that differences in magnetic behaviour may have stemmed from differences in $Fe^{II}N_6$ geometry, intermolecular interactions and chemical pressure.

Compounds **5a**, **5b** and **5c** were made in acetonitrile while the previously reported complexes α-$[Fe^{II}(DBB)_2(NCS)_2]$ and β-$[Fe^{II}(DBB)_2(NCS)_2]$ were made in ethanol. It is interesting to note that complex **5b**, which contains no solvent in the outer coordination sphere is not isostructural to either of the non-solvated complexes α-$[Fe^{II}(DBB)_2(NCS)_2]$ or β-$[Fe^{II}(DBB)_2(NCS)_2]$. Complexes α-$[Fe^{II}(DBB)_2(NCS)_2]$ and β-$[Fe^{II}(DBB)_2(NCS)_2]$, were found by Ross *et al*.,[5a] to show intermolecular interactions largely consisting of edge-to-face CH...π or face-to-face π-stacking interactions between aromatic moieties of the DBB ligand, therefore it is surprising that the present non-solvated analogue, **5b**, did not show similar interactions. The study by Ross *et al*.,[5a] interestingly found that the most salient difference between the α- and β-analogues was the manner in which the dibenzylamino moieties of the DBB ligands were oriented, and this was thought to provide the differences in magnetic behaviour between the two polymorphs. Similar results were found in the present study where the three different crystalline products of **5** each exhibit markedly different orientations of their dibenzylamino groups (Figure 7).

In the case of the isostructural DBB compounds **5c** and **6**, differing only in the NCX group, they represent a good pair of compounds in which to compare the magnetic properties. Their magnetic features (Figs. 9c and 9d) are described above and are generally similar. After heating from low temperatures up to 350 K (**5c**) and 400 K (**6**), followed by cooling, both complexes show the same $\chi_M T$ values down to 320 K (**5c**) and 350 K (**6**) which we believe is due to loss of MeCN solvent molecules from the crystal lattice. The $T_{1/2}$ values of **5c** (330 K) and **6** (360 K) are consistent with different ligand field strengths of the NCSe and $NCBH_3$ ligands, as discussed below. Intermolecular interactions are of the C..CH type (Table 2) and thus are weak. Ligand disorder in **5c** might contribute to cooperativity but we have no evidence for this.

Intermolecular π-π and other interactions and spin crossover

We turn now to spin states and cooperativity (hysteresis/abruptness) of spin transitions and qualitative relations to intermolecular and crystal packing interactions in these $FeL_2(NCX)_2$ complexes. A survey of all intermolecular interactions exhibited by complexes described here, which will contribute to spin states and to SCO cooperativity, is given in Table 2. Other comments on intermolecular ointeractions are also given under other headings such as Solvent effects. At first sight, there do not appear to be any particular interactions, or combinations of interactions, in Table 2, that consistently relate to abrupt transitions/stronger cooperativity. Furthermore, in regard to the initial aim of using the present aromatic-substituted s-triazine ligands to enhance π-π stacking which, in turn, would enhance cooperativity in the SCO compounds, we have been thwarted by HS behaviour in the DTT complexes **1** and **2**, with the other complexes, apart perhaps for **7**, not displaying π-π stacking. The DBNT complex **7** also shows a HS structure at 100 K but the magnetism shows hints of a partial crossover at ~160 K. It seemed that since the SCO complexes **3** to **6** display H-bonding and π-CH interactions (Table 2), π-π interactions play a minor role in affecting cooperativity in the present compounds.

However, perusal of other SCO systems in which π-π interactions play a key role include the bis-tridentate iron(III) *N*-quinolinyl salicylaldimine families, $[Fe(qsal\text{-}X)_2]^+$, where X = H, Cl, Br, I.[14,15,16] A common supramolecular motif in these families is the formation of 1D chains via π-π interactions between planar qsal ligands within the Fe cations, with secondary interactions between chains, such as X...π, CH...O, CH…π or aromatic..aromatic P4AE, in some cases, leading to 2D sheets or pseudo-3D networks. The 1D intermolecular chains were found to be so robust that Harding *et al.* felt that they may be used in the control and design of new $[Fe(qsal\text{-}X)_2]^+$ SCO materials.[14]

Applying the ideas developed for qsal-X supramolecular chemistry to the present complexes **1** and **2** (HS) and **5a** and **5b** (SCO), has led to interesting structure-magnetism correlations. The π- π interactions in **1** and **2** that connect Fe centres into 1D chains are strong and lead to rigid environments around the Fe centres thus preventing the Fe centres from re-orienting during a spin change, hence they remain HS (Figure 13). Furthermore, the CH.. π interactions that link the chains into sheets in **1** and **2** (ESI; Figs. S1 and S7) do not allow the Fe sites to communicate and exhibit spin changes throughout the structure. In contrast, the C-H..π interactions forming 1D motifs in **5b** (ESI, Figs. S5 and S7) are more flexible and provide space for the Fe centres to shrink or expand to reach LS or HS states. In **5a**, the offset π-π interactions between benzyl aromatic rings, forming 1D chains (ESI, Fig. S5), do not involve the coordinating dpa moiety, thus leaving flexible space around the Fe centres. Together with the offset π- π interactions between chains, this promotes spin crossover, as observed crystallographically (*vide infra)*. The MeCN solvate molecules in **5a** probably play a space filling role rather than transmitting intermolecular interactions.

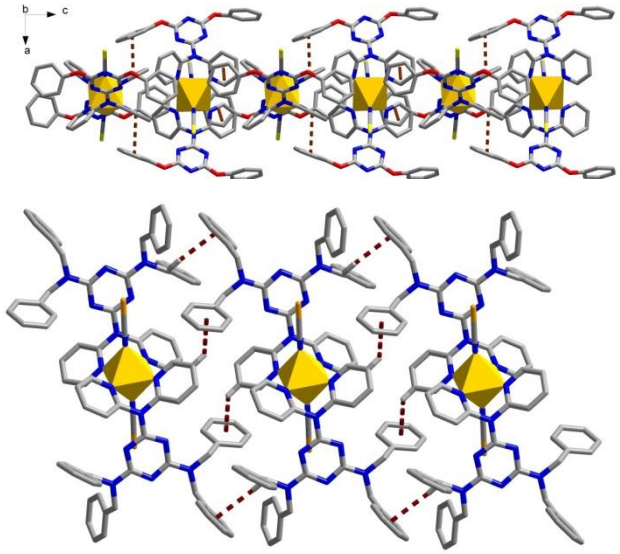

Figure 13. π-π interactions between the pyridyl and the phenyl rings in compound **1** viewed along the *b* axis (a), and the C-H..π interactions in compound **5b** that link the Fe centres into 1D chains (b). Temperature 123 K.

Ligand field considerations

In the case of the SCO compounds **1**-**7** the NCX⁻ anions are coordinated directly to the Fe(II) centre, *i.e*., the NCX⁻ anions in this case are a direct co-determinant of the ligand field strength at the metal centre. The DBT complexes follow the ligand field strengths expected for their respective NCX bonded complexes (*viz.* NCS <NCSe). It was more difficult to make such comparisons in the DBB series in which compound **5** exhibits three polymorphs/solvates, with only **5c** being isostructural to

the $NCBH_3$ (**6**) analogue. Ignoring, for the moment, the solvate molecule(s), if NCX is kept constant, the *s*-triazine-dipyridylamino-based ligand variation yields the ligand-field variation DTT < DBNT < DBT for NCS and DTT < DBT < DBB for NCSe.

Solvent effects

Non-coordinated solvent molecules are known to affect crystal packing and intermolecular interactions and, hence, SCO properties. Attempts were made to collect structural data for complex **5a** in both the solvated and desolvated state, however raising the diffraction temperature to 288 K was not sufficient enough to remove solvent from the crystal lattice. Less gentle techniques at removing lattice solvent for complex **5a**, including mild heating, resulted in the loss of crystallinity thus rendering further diffraction studies unachievable.

For complex **6**, the slightly different pathway of magnetic susceptibility on the cooling mode we think is attributed to the loss of lattice solvent at room temperature, rather than to hysteresis or to HS trapping, so that a gradual SCO is observed.

It was surprising to see that complexes **3** and **4** crystallise, reproducibly and in different space groups, as a dimethanol solvate and a non-solvate, respectively, while being made under the same methanolic conditions. The intermolecular interactions found for these complexes are not strong and so it is not entirely clear why these complexes crystallise in the form they do. Using similar $[Fe^{II}(L)_2(NCX)_2]$-type systems, similar behaviour has been observed previously,[7] although differences in packing and solvation between analogous complexes can usually be explained by strong intermolecular interactions.

The solvent molecules of H_2O found in complexes **1** and **2** are thought to arise from using the hydrated metal salt or the use of methanol which may contain small amounts of water. The O3 atom from the solvent H_2O molecule in **1** and **2** H-bonds to N-atoms of the *s*-triazine and this interaction is probably responsible for the incorporation of H_2O in the crystal lattice.

Solvates of **1** and **2** have previously been reported,[6b] and have been found to exhibit SCO behaviour. The difference in magnetic behaviour between **1** and **2** and their solvate complexes $[Fe(DTT)_2(NCS)_2]\cdot 2CH_2Cl_2$ and $[Fe(DTT)_2(NCSe)_2]\cdot 4CH_2Cl_2\cdot 4CH_3OH$, likely stems from the incorporation of solvent molecules and the nature of the packing of complexes within the crystal lattice. For example, Gamez *et al*. have pointed out that in $[Fe(DTT)_2(NCS)_2]\cdot 2CH_2Cl_2$ the Fe(II)-DTT centres interact weakly through CH…O and CH…π contacts producing a supramolecular 1D chain.[6b] Furthermore, the crystal packing of $[Fe(DTT)_2(NCSe)_2]\cdot 4CH_2Cl_2\cdot 4CH_3OH$ reveals the formation of a 1D chain of Fe(II) complexes that are connected by parallel-displaced π…π interactions involving the phenyl ring.

Comparing the supramolecular interactions in **1** and **2** to those of Gamez' complexes, it is interesting to note that **1** and **2** also form 1D supramolecular chains, although the intermolecular contacts forming these chains differ to those in the Gamez species.[6b] Because the degree of cooperativity within a complex often dictates the nature of the spin transition, it is surprising that complexes **1** and **2** remain HS, despite showing similar supramolecular interactions to those of Gamez' complexes. Additionally, because the ligand field environment around the Fe^{II} centres of **1** and **2** should be almost identical to that of $[Fe(DTT)_2(NCS)_2]\cdot 2CH_2Cl_2$ and $[Fe(DTT)_2(NCSe)_2]\cdot 4CH_2Cl_2\cdot 4CH_3OH$, the influence of entities existing outside the first coordination sphere and packing arrangements affecting the magnetic character are exemplified.

The structural comparisons and differences drawn between complexes **1**, **2** and the complexes $[Fe(DTT)_2(NCS)_2]\cdot 2CH_2Cl_2$ and $[Fe(DTT)_2(NCSe)_2]\cdot 4CH_2Cl_2\cdot 4CH_3OH$ highlight the influence that the hydrogen bonding and intermolecular interactions have on the communication pathways for the cooperative interactions propagating through the lattice. One possibility here is that stronger hydrogen bonding, from replacing the chlorinated solvents with water, in **1** and **2**, may lead to a stronger framework, which pins the Fe(II) centres in place and does not allow shrinkage upon HS◊LS conversion.

Octahedral distortions

For SCO complexes, the octahedral distortion around the crossover centre, measured by Σ and Θ, decreases as the spin transition occurs to form the LS state. Σ values of ~65° in the HS form have previously been reported for $[Fe^{II}(L)_2(NCX)_2]$-type SCO complexes, including early work on $[Fe^{II}(phen)_2(NCS)_2]$ and $[Fe^{II}(bpy)_2(NCS)_2]$ (where phen = 1,10-phenanthroline and bpy = 2,2'-bipyridine) complexes.[9] These values are relatively larger than the values calculated for the complexes measured here. The smaller values for Σ, here, could result from the flexible nature of the chelating 2,2'-dipyridylamino substituent when compared to the more rigid coordination motifs provided by phen and bpy, this is supported by the lower Σ values obtained for $[Fe^{II}(py)_4(NCS)_2]$-type systems.[9] Furthermore, similar Σ values using similar *s*-triazine-dipyridylamino-based ligands have been found in our previous work[5d] and by Gamez *et al*.[6b]

In the present study, only the crystal structure of complex **5a** was collected in both the HS and LS states, therefore ΔΣ (where ΔΣ is the difference between Σ in the HS state and the LS state, given as a percentage of Σ at HS) has been calculated for this complex *viz* ~31%, reflecting a strong distortion from LS to HS.

The distortion of the FeN_6 octahedron has also been linked to both $T_{1/2}$ and the abruptness of SCO. Previously, larger values of Θ at HS have been linked to more abrupt SCO and a larger ΔΘ (where ΔΘ is the difference in Θ in the HS state and the LS state) have been linked to lower $T_{1/2}$ values.[10] For complex **5a** relatively low values for both Θ at HS and ΔΘ have been calculated (74º and 31º, respectively) which confirm the occurrence of a gradual SCO with a relatively high $T_{1/2}$ value. These values are similar in magnitude to those of analogous Fe^{II}-dipyridylamino-based SCO systems.[6b]

LIESST effect

The photomagnetic properties of complexes **3** and **4** have been recorded. Complex **4** did not present any LIESST effect. However, complex **3** did exhibit both LIESST and reverse-LIESST which allowed the *T*(LIESST) temperature (42K) to be determined. Regarding the *T*(LIESST)/$T_{1/2}$ values, compound **3** belongs to the a T_0 = 100 K line in the *T*(LIESST) *vs.*$T_{1/2}$ database reported by Létard *et al*.[11,12] This line encompasses many $[Fe(L)_2(NCX)_2]$ examples. According to this database, a compound belonging to the T_0= 100 K line with a $T_{1/2}$ of 275 K, as in compound **4**, should exhibit a *T*(LIESST) value of around 15 K which is hardly observable on the SQUID magnetometer and could explain why compound **4** shows no LIESST effect. Compounds **1-7** as well as the compounds reported by Gamez[6b] follow this trend.

The parameters obtained from the relaxation kinetic analysis (25-40 K) of **3** *viz*. activation energy E_a of 165 cm^{-1} and k_∞ of 0.25 s^{-1}, are typical of such mononuclear species and indicative of weak cooperativity.[11,12] The presence of two relaxation processes observed in the *T*(LIESST) and the kinetics curves could indicate that short range and long range interaction co-exist in these materials. Regarding the structures, many contacts are present leading to layer topologies. Therefore, intra-layers and inter-layers interactions could take place with different strength.

Conclusions

Four dipyridylamino-based ligands have been incorporated into seven mononuclear Fe^{II} coordination complexes. The degree of flexibility and steric bulk of each ligand, in combination with their ligand field strengths, and of the terminal NCX^- ligands, has been investigated in relation to the nature of the SCO behaviour observed for each complex.

Magnetostructural investigations on complexes presented here

further exemplify the complexity of factors influencing the magnetic character. These factors include the molecular conformation, the first coordination sphere geometry and intermolecular interactions, and the present results show the diversity of the ways in which these factors may operate. For example, the complexes **5a** and **5c** emphasise the significant contributions packing arrangements can have on the observed SCO behaviour. In addition, comparisons between complexes **1** and **2** to reported analogues[6b] demonstrate the influence solvation bears upon the packing arrangement within the crystal lattice which, in turn, influence the magnetic behaviour. **1** and **2**, in this study were found to remain HS over the temperature range 2 - 300 K, whereas previous analogues, exhibiting differences in packing, have been found to show SCO behaviour. We have given strong arguments, above, to explain the HS behaviour in **1** and the SCO behaviour of **5b**, in terms of the strength and rigidity in 1D π-π chains compared to the more flexible inter-chain interactions. In general, however, despite the systematic way that the dipyridylamino-triazine-based ligand and the NCX^- ligand have been varied here and in previous work, the influence of the solvate molecules in the second coordination sphere remains the most difficult to pin down with certainty.

Finally, compared to the control achieved in Fe(III) qsal-X structures and magnetism (*vide supra)*,[14,15,16] we do not yet have similar control in designing SCO examples of Fe(II) using the present substituted-dipyridylamine-triazine (L) ligands. Even though we,[5,7] and Gamez and coworkers,[6] obtain very interesting crystalline SCO $[Fe(II)(L)_2(NCX)_2]$ species, in which structure-magnetism correlations of the type described here can be made, in considerable detail, we do not yet have the control in, for example, inducing π-π interactions, nor can we predict the presence or nature of included solvate molecules. Thus obtaining HS species, rather than SCO compounds, remains a common occurrence even when sensible variations are made in the NCX groups and/or the L groups.

Experimental Section

General

All reagents and solvents were purchased from Sigma-Aldrich and used as received. Infrared spectra were measured on a Bruker Equinox 55 FT-IR fitted with a 71Judson MCT detector and Specac 'Golden Gate' diamond ATR. Mass spectrometry analyses were performed using electrospray ionization mass spectra (ESI-MS) and were recorded on a Micromass (now Waters) ZMD with Waters alliance e2695 HPLC system for automatic sample injections. MeOH was the mobile phase and had a flow rate of 100 µL/min. Microanalyses were performed by Campbell Microanalytical Laboratory, Department of Chemistry, University of Otago, Dunedin, New Zealand. Variable temperature magnetic susceptibility data were collected using either a Quantum Design MPMS 5 Superconducting Quantum Interference Device (SQUID) magnetometer or a MPMS XL-7 SQUID magnetometer, with a scan speed of 10 K/min followed by a one minute wait after each temperature change. In cases when steps were less than 10 K the target temperature is reached in less than 1 min; hence it takes longer to stabilise at the target temperature. Samples were dispersed in Vaseline to prevent torquing due to anisotropy of the high spin states.

X-ray crystallographic measurements on **5b** were performed at 123(2) K using a Bruker Smart Apex X8 diffractometer with Mo Kα radiation, λ = 0.71073 Å. Single crystals were mounted on a glass fibre using oil. The data collection and integration were performed within SMART and SAINT+ software programs, and corrected for absorption using the Bruker SADABS program.[17]

X-ray crystallographic measurements on **1**, **2**, **3**, **4**, **5c**, **6** and **7** were collected at the Australian Synchrotron using the MX1 beam-line operating at ~16 keV (λ = 0.71073 Å). The collection temperature was maintained at specified temperatures using an open-flow N_2 cryostream. Data were collected using the Blue Ice software.[18] Initial data processing was carried out using the XDS package.[19]

X-ray crystallographic measurements on **5a** were collected on an Oxford Gemini Ultra diffractometer at 123(2) K with Cu-Kα radiation (*λ* = 1.5418 Å). Crystals were mounted on glass fibres in a small amount of oil. Diffraction data analysis was performed using CrysAlisPro, Oxford Diffraction Ltd., Version 1.171.34.36. Empirical absorption correction was performed using spherical harmonics, implemented in the SCALE3 ABSPACK scaling algorithm.[20]

Crystallographic data and refinement parameters for **1**-**7**, given in Table 3, were solved by direct methods (SHELXS-97), and refined (SHELXL-97) by full least-squares on all F^2 data.[21] All other non-hydrogen atoms in **1**–**7** were refined anisotropically and all hydrogen atoms were placed in calculated positions.

Complexes **1** and **2** are isostructural and so their crystallographic data were treated the same way. **1** and **2** contain a half solvent H_2O molecule. The O3 atom sat on a four-fold rotary inversion axis and therefore the asymmetric unit basically contains half a complex and quarter of a water molecule, which gives a %hydration of 50%. O3 was left isotropic and no hydrogen atoms have been placed on it.

Complex **3** was refined as a racemic twin, using SHELX-97,[21] and a BASF refined to 0.55292 was obtained.

Complexes **5c** and **6** are isostructural and so their crystallographic data were treated the same way. The structure of complexes **5c** and **6** contain disorder in two phenyl rings of the DBB ligand. The CH_2 arm containing C16 and the entire ring containing C17 to C22 were disordered over two positions (giving C16', C17, C18', C19', C20', C21' and C22'), with each assigned to 50% occupancy.The second site of disorder occurs in the ring incorporating C31 to C36; here atoms C34, C35 and C36 were disordered over two positions (giving C34', C35' and C36'). Each of these atoms was assigned to 50% occupancy. The ISOR restraints were placed on atoms C16 and C16'.

CCDC numbers 1037551-1037560. These data can be obtained free of charge from The Cambridge Crystallographic Data Centre via www.ccdc.cam.ac.uk/datarequest/cif.

Photomagnetic characterisation for compound **3** was carried out at CNRS, Université de Bordeaux, ICMCB, with a Spectrum Physics Series 2025 Kr+ laser coupled through an optical fibre into the cavity of an MPMS-55 Quantum design SQUID magnetometer operating at 2 T. Samples were prepared as a thin layer (*ca.* 0.1 mg) to promote full penetration of the irradiated light. The sample weight was obtained by comparing its thermal spin transition behaviour with an accurately weighed sample. The sample was first slowly cooled to 10 K by ensuring that potential trapping of HS species at low temperatures did not occur. Irradiation to photosaturation was carried out a number of times at different wavelengths to determine which source was most efficient at a power intensity of 5 mW/cm^2 (to prevent warming of the sample). Samples were then cooled to 10 K and irradiated with green light (*λ*= 532 nm) until photosaturation was reached. Then, in the absence of irradiation, the temperature was increased at a rate of 0.3 $K\ min^{-1}$. The extreme of the $\delta\chi MT/\delta T$ *vs.T* plot gave the *T*(LIESST) value, defined as the temperature for which the light-induced HS information is erased. At 10 K, compound **3** was again irradiated to photosaturation, and in the absence of irradiation the relaxation kinetics were measured.

Table 3. Crystal data and refinement details. [a] $R_1 = \sum||F_o| - |F_c||/\sum|F_o|$. [b] $wR_2 = \{\sum[w(F_o^2\sum F_c^2)^2]/\sum[w(F_o^2)]\}^{1/2}$.

Compound	1	2	3	4	5a (123K)	5a (288K)	5b
Formula*	$C_{52}H_{36}N_{14}O_{4.5}Fe_1S_2$	$C_{52}H_{36}N_{14}O_{4.5}Fe_1Se_2$	$C_{58}H_{40}Fe_1N_{18}O_6S_2$	$C_{56}H_{32}Fe_1N_{18}O_4Se_2$	$C_{88}H_{78}Fe_1N_{20}Se_2$	$C_{88}H_{78}Fe_1N_{20}Se_2$	$C_{84}H_{72}N_{18}Fe_1Se_2$
Mw (g mol^{-1})	1048.92	1142.72	1205.05	1234.77	1629.47	1629.47	1547.37
T (K)	100	100	100	100	123	288	123
Crystal system	Tetragonal	Tetragonal	Orthorhombic	Triclinic	Triclinic	Triclinic	Monoclinic
Space group	$P4_2/n$	$P4_2/n$	$Pca2_1$	P-1	P-1	P-1	$P2_1/n$
Z	4	4	4	1	1	1	2
a (Å)	17.958(3)	17.975(3)	34.295(7)	8.3370(17)	11.6341(5)	11.7947(11)	10.297(2)
b (Å)	17.958(3)	17.975(3)	8.7790(18)	9.2280(18)	12.1539(6)	12.5435(12)	39.153(8)
c (Å)	14.707(3)	14.816(3)	19.149(4)	17.810(4)	15.22332(5)	15.2482(12)	10.359(2)
α (°)	90.00	90.00	90.00	89.38(3)	84.630(4)	83.767(8)	90.00
β (°)	90.00	90.00	90.00	89.60(3)	80.249(3)	80.169(7)	119.44(3)
γ (°)	90.00	90.00	90.00	72.00(3)	64.199(4)	63.341(9)	90.00
V (Å^3)	4742.9(19)	4787.1(14)	5765(2)	1303.3(5)	1909.49(14)	1985.2(3)	3637.2(13)
ρ_{calc} (g cm^{-3})	1.458	1.590	1.388	1.573	1.417	1.363	1.413
μ (mm^{-1})	0.471	1.900	0.402	1.754	1.213	1.167	1.269
Measured/independent Reflections (R_{int})	83655/6122(0.1219)	78661/5169(0.1971)	78713/15821(0.0717)	29544, 7707(0.0301)	23321/12190(0.0364)	23387/12627(0.0315)	36791/9809(0.0447)
Observed reflections [I > 2σ(I)]	4319	4582	13260	6983	8724	6687	8892
R_1[a], wR_2[b][I > 2σ(I)]	0.0553, 0.1365	0.0568, 0.1540	0.0514,0.1366	0.0362,0.0902	0.0469, 0.1031	0.0560, 0.1076	0.0375, 0.0966
R_1, wR_2 (all data)	0.0861, 0.1549	0.0615, 0.1575	0.0645,0.1457	0.0408, 0.0932	0.0779, 0.1193	0.1234, 0.1381	0.0425, 0.1104
Goodness-of-fit on F^2	1.058	1.050	0.989	1.053	1.030	1.010	1.095

Compound	5c	6	7
Formula*	$C_{88}H_{78}Fe_1N_{20}Se_2$	$C_{88}H_{84}B_2Fe_1N_{20}$	$C_{44}H_{30}C_{12}Fe_1N_{16}O_4S_2$
Mw (g mol^{-1})	1629.47	1499.21	1037.71
T (K)	100	100	100
Crystal system	Triclinic	Triclinic	Triclinic
Space group	P-1	P-1	P-1
Z	1	1	1
a (Å)	8.6200(17)	8.5960(17)	8.7730(18)
b (Å)	15.052(3)	15.099(3)	11.732(2)
c (Å)	15.250(3)	15.225(3)	12.310(3)
α (°)	92.78(3)	92.97(3)	81.07(3)
β (°)	97.94(3)	98.20(3)	71.62(3)
γ (°)	92.83(3)	92.72(3)	88.73(3)
V (Å^3)	1954.2(7)	1954.0(7)	1187.3(4)
ρ_{calc} (g cm^{-3})	1.381	1.265	1.451
μ (mm^{-1})	1.184	0.253	0.579
Measured/independent Reflections (R_{int})	34893/8975(0.1632)	35155,9018(0.1664)	19108/4876(0.0298)
Observed reflections [I > 2σ(I)]	5012	5090	4370
R_1[a], wR_2[b][I > 2σ(I)]	0.0699, 0.1468	0.0788,0.1717	0.0427, 0.1156
R_1, wR_2 (all data)	0.1491, 0.1838	0.1552,0.2099	0.0477, 0.1197
Goodness-of-fit on F^2	1.015	1.046	1.065

Ligand and Precursor Syntheses

The synthetic procedure for DTT was the same as that reported in T. Ross, Ph.D. Thesis, Monash University, 2010.[5d] A modified procedure has also appeared in the literature.[6b] The synthetic procedure for DBB used the reported method.[5a]

BBT (precursor to DBT) - 4,4'-((6-chloro-1,3,5-triazine-2,4,-diyl)bis(oxy))dibenzonitrile

Cyanuric chloride (3.0 g, 16.3 mmol) and *N,N'*-diisopropylethylamine (DIPEA) (3 ml) were dissolved in 100 ml tetrahydrofuran and cooled to -30ºC with stirring. Separately, 4-hydroxybenzonitrile (3.8 g, 31.9 mmol) was dissolved in 100 ml tetrahydrofuran and this solution was added dropwise to the stirring cyanuric chloride/DIPEA solution over the course of two hours. After complete addition, the resultant solution was allowed to reach ambient temperature and left stirring under N_2 overnight. After this time, the solution was filtered and 100 ml deionised water was added to the filtrate. Tetrahydrofuran was then removed *in vacuo* and the solution was then extracted with chloroform (2 × 50 ml). The combined organic extracts were reduced *in vacuo* to a point where precipitate began to appear. Hexane was then added to this solution to form a white powder which was filtered. M_w 349.73; Yield 2.90 g (50 %); ^{1}H NMR (400 MHz, [D$_6$]DMSO): δ 7.808 (4H, d, J = 8.8 Hz), 7.349 (4H, d, J = 8.8 Hz) ppm; ^{13}C NMR (400 MHz, [D$_6$]DMSO): δ 159.730, 134.306, 134.119, 122.541, 119.138, 116.383, 103.719 ppm; IR: ῡ = 3266 (s), 2231 (s), 1601 (s), 1585 (s), 1507 (s), 1439 (s), 1364 (m), 1282 (s), 1220 (s), 1165 (s), 1105 (s), 834 (s), 700 (m) cm^{-1}; ESI-MS found [M+Na]$^+$ peak at *m/z* 372.2

DBT - 4,4'-((6-(di(pyridine-2-yl)amino)-1,3,5-triazine-2,4-diyl)bis(oxy))dibenzonitrile

BBT (0.77 g, 2.2 mmol), 2,2'-dipyridylamine (0.72 g, 2.6 mmol) and 2 ml DIPEA were dissolved together in 30 ml MeCN. The solution was refluxed with stirring for five days. After this time, 50 ml H_2O was added to the solution and the MeCN removed *in vacuo*. The product was then extracted with 2 × 50 ml $CHCl_3$ and the combined organic extracts reduced *in vacuo* to give a pale brown solid. The product was then purified via column chromatography to produce a white powder (SiO_2 3.5:0.5 DCM:THF (v/v), R_f = 0.66). M_w 484.47;Yield 0.86 g (80 %); ^{1}H NMR (400 MHz, [D$_6$]DMSO): δ 8.344 (2H, ddd, J = 0.8, 2.0, 4.8 Hz), 7.932 (4H, d, J = 8.8 Hz), 7.884 (2H, ddd, J = 1.6, 7.2, 9.2 Hz), 7.587 (2H, dm, J = 9.2 Hz), 7.488 (4H, d, J = 9.2 Hz), 7.287 (2H, ddd, J = 0.8, 4.8, 7.2) ppm;^{13}C NMR (400 MHz, [D$_6$]DMSO): δ 171.097, 167.525, 154.813, 153.845, 148.348, 137.704, 133.821, 122.939, 122.820, 121.924, 118.295, 108.421 ppm; IR: ῡ = 3064 (w), 2227 (s), 1587 (s), 1543 (s), 1490 (s), 1463 (s), 1431 (m), 1359 (s), 1301 (m), 1235 (s), 1204 (s), 1167 (s), 1015 (m), 852 (w), 807 (w), 777 (w), 746 (w), 683 (w) cm^{-1}; ESI-MS [M+H]$^+$ peak found at *m/z* 485.0, [M+Na]$^+$ peak found at *m/z* 506.9. $C_{27}H_{16}N_8O_2$:calcd C 66.94, H 3.33, N 23.13; found C 66.74, H 3.41, N 22.74.

Mono-BBT (precursor to DBNT)–4,4'-((4,6-dichloro-1,3,5-triazin-2-yl)oxy)benzonitrile

4-((4,6-dichloro-1,3,5-triazin-2-yl)oxy)benzonitrile was synthesised following the same method as that for ,4'-((6-chloro-1,3,5-triazine-2,4,-diyl)bis(oxy))dibenzonitrile, however it was eluted from the column at R_f = 0.52. M_w 267.07;Yield 48 mg (8 %);^{1}H NMR (400 MHz, [D$_6$]DMSO): δ 8.037 (2H, d, J = 8.8 Hz), 7.592 (2H, d, J = 8.8 Hz) ppm; IR: ῡ = 3264 (br), 2957 (w), 2927 (m), 2853 (m), 2228 (s), 1611 (s), 1586 (s), 1530 (s), 1511 (s), 1440 (s), 1417 (s), 1359 (s), 1298 (s), 1283 (s), 1262 (s), 1236 (s), 1196 (s), 1164 (s), 1103 (m), 1063 (w), 1007 (m) 876 (m), 833 (m), 807 (m), 771 (m), 732 (m), 691 (w) cm^{-1}; $C_{10}H_4N_{20}O_1Cl_2$: cald C 44.97, H 1.51, N 20.98; found C 45.10, H 1.46, N 20.95.

DBNT - 4-((4-chloro-6-(di(pyridin-2-yl)amino)-1,3,5-triazin-2-yl)oxy)benzonitrile

4-((4,6-dichloro-1,3,5-triazin-2-yl)oxy)benzonitrile (0.90 g, 3.37 mmol), and 2,2'-dipyridylamine (0.58 g, 3.37 mmol) and 2 ml DIPEA were dissolved in 30 ml of MeCN and the solution refluxed for two weeks. After this time, the solvent was removed *in vacuo* and the product, a dark brown sticky solid, was washed with 30 ml H_2O and extracted with $CHCl_3$ (2 × 30 ml). The combined extracts were reduced *in vacuo* to give a dark brown semi-solid. 10 ml $CHCl_3$ was then added, along with 50 ml hexane and the solution brought to boiling with stirring for 15 mins. The yellow solution was decanted off and left to evaporate (leaving a sticky brown semi-solid). Once dried, the yellow powdered product was washed with 20 ml MeOH to give a clean white powder and yellow solution. The powder was filtered off and washed with a further 10 ml MeOH. M_w 401.81; Yield 0.69 g (51 %);^{1}H NMR (400 MHz, [D$_6$]DMSO): δ 8.40 (2H, ddm, J = 4.8, 1.2 Hz), 7.969 (2H, m), 7.933 (2H, dm, J = 2.0 Hz), 7.656 (2H, dm, J = 8.4 Hz); 7.522 (2H, m), 7.351 (2H, ddd, J = 6.4, 4.8, 6.4 Hz) ppm; ^{13}C NMR (400 MHz, [D$_6$]DMSO): δ 170.508, 169.647, 166.657, 154.593, 153.592, 148.580, 138.070, 133.950, 122.880, 122.795, 122.405, 118.248, 108.710 ppm; IR: ῡ= 2224 (s), 1584 (s), 1554 (s), 1522 (s), 1490 (s), 1461 (s), 1430 (s), 1364 (s), 1314 (s), 1290 (s), 1271 (s), 1250 (s), 1228 (s), 1195 (s), 1166 (s), 1118 (s), 1052 (s), 1018 (m), 985 (s) 965 (m), 939 (m), 855 (m), 830 (s), 801 (s), 779 (s), 744 (m), 686 (m), 670 (m), 622 (m) cm^{-1}; ESI-MS [M+H]$^+$ peak found at *m/z* 402.2, [M+Na]$^+$ peak found at *m/z* 424.2 $C_{20}H_{12}N_7O_1Cl_1$: calcd C 59.78, H 3.01, N 24.40; found C 59.58, H 2.99, N 24.05.

Metal Complex Syntheses

***trans*-[Fe^{II}(DTT)$_2$(NCS)$_2$]·(H$_2$O)$_{1/2}$ (1)**

DTT (15 mg, 0.034 mmol) was dissolved in 4 ml methanol. Separately, $Fe(ClO_4)_2{\cdot}xH_2O$ (4.3 mg, 0.017 mmol), NaNCS (2.8 mg, 0.034 mmol) and 5 mg ascorbic acid were dissolved in 4 ml methanol. Following 30 mins of stirring, the methanolic Fe^{II}/NCS solution was added dropwise to the solution of ligand to produce a pale yellow solution. This solution was then filtered and the filtrate left to slowly evaporate. Over the course of two days small yellow crystals had formed. M_w 1048.92; Yield 6 mg (33 %); IR:ῡ= 1594 (s), 1577 (s), 1551 (s), 1483 (s), 1464 (s), 1436 (s), 1364 (s), 1307 (s), 1281 (m), 1244 (s), 1196 (s), 1159 (w), 1071 (s), 1011 (s), 908 (s), 876 (w), 826 (s), 807 (m), 789 (s), 759 (s), 713 (s), 684 (s), 640 (s) cm^{-1}; $C_{52}H_{36}Fe_1N_{14}O_4S_2$: calcd C 60.0, H 3.49, N 18.84; found C 59.7, H 3.76, N 18.79.

***trans*-[Fe^{II}(DTT)$_2$(NCSe)$_2$]·(H$_2$O)$_{1/2}$ (2)**

DTT (15 mg, 0.034 mmol) was dissolved in 4 ml methanol. Separately, $Fe(ClO_4)_2{\cdot}xH_2O$ (4.3 mg, 0.017 mmol), KNCSe (4.8 mg, 0.034 mmol) and 5 mg ascorbic acid were dissolved in 4 ml methanol. Following 30 minutes of stirring, the the methanolic Fe^{II}/NCSe solution was added dropwise to the solution of ligand to produce a pale yellow solution. This solution was then filtered and the filtrate left to slowly evaporate. Over the course of two days small yellow crystals had formed. M_w 1142.72; Yield 7 mg (36 %); IR: ῡ = 1594 (s), 1552 (s), 1483 (s), 1463 (s), 1366 (s), 1306 (s), 1244 (m), 1195 (w), 1160 (s), 1124 (s), 1011 (m), 908 (s), 875 (s), 806 (s), 789 (s), 760 (m), 727 (s), 684 (s), 641 (s) cm^{-1};$C_{52}H_{36}Fe_1N_{14}O_4Se_2$: calcd C 55.04, H 3.20, N 17.28; found C 54.88, H 3.22, N 16.95.

***trans*-[Fe^{II}(DBT)$_2$(NCS)$_2$]·2MeOH(3)**

DBT (15 mg, 0.031 mmol) was dissolved in 4 ml methanol. Separately, NaNCS (2.5 mg, 0.031 mmol), $Fe(ClO_4)_2{\cdot}xH_2O$ (3.9 mg, 0.015 mmol) and 5 mg ascorbic acid were dissolved in 4 ml methanol. Following one hour of stirring the the methanolic Fe^{II}/NCS solution was added dropwise to the solution of ligand to produce a pale yellow solution. This solution was filtered and the filtrate left to slowly evaporate. M_w 1205.03; Yield 12 mg (66 %); IR: ῡ = 3065 (w), 2229 (m), 2069 (s), 1611 (s), 1583 (s), 1555 (s), 1498 (s), 1468 (s), 1440 (s), 1367 (s), 1311 (s), 1284 (s), 1249 (s), 1205 (s), 1168 (s), 1079 (s), 1016 (s), 884 (w), 861 (w), 835 (w), 807 (w), 785 (w), 758 (w), 672 (w), 658 (w) cm^{-1}; $C_{56}H_{32}Fe_1N_{18}O_4Se_2$: calcd C 54.47, H 2.61, N 20.42; found C 54.49, H 2.73, N 20.18.

***trans*-[Fe^{II}(DBT)$_2$(NCSe)$_2$](4)**

DBT (15 mg, 0.031 mmol) was dissolved in 4 ml methanol. Separately, KNCSe (4.4 mg, 0.031 mmol), $Fe(ClO_4)_2{\cdot}xH_2O$ (3.9 mg, 0.015 mmol) and 5 mg ascorbic acid were dissolved in 4 ml methanol. Following one hour of stirring the the methanolic Fe^{II}/NCSe solution was added dropwise to the solution of ligand to produce a pale yellow solution. This solution was filtered and the filtrate left to slowly evaporate. M_w 1234.77; Yield 12 mg (64 %); IR: ῡ = 3020 (w), 2227 (m), 2102 (m), 2072 (s), 1568 (s), 1564 (s), 1547 (s), 1497 (s), 1482 (s), 1468 (s), 1439 (s), 1409 (s), 1362 (s), 1311 (s), 1249 (s), 1221 (s), 1207 (s), 1157 (s), 1082 (s), 1017 (m), 839 (w), 805 (w), 778 (w), 755 (w), 657 (w) cm^{-1}; $C_{56}H_{32}Fe_1N_{18}O_4Se_2$: calcd C 58.95, H 2.83, N 22.10; found C 58.58, H 2.86, N 21.85.

***trans*-[Fe^{II}(DBB)$_2$(NCSe)$_2$]·2(MeCN) and *trans*-[Fe^{II}(DBB)$_2$(NCSe)$_2$] (5a, 5b and 5c)**

DBB (20 mg, 0.031 mmol) was dissolved in 4 ml methanol. Separately, KNCSe (4.5 mg, 0.031 mmol), $Fe(ClO_4)_2{\cdot}xH_2O$ (4 mg, 0.015 mmol) and 5 mg ascorbic acid were dissolved in 4 ml acetonitrile. Following one hour of stirring the the methanolic Fe^{II}/NCSe solution was added dropwise to the solution of ligand to produce an orange solution. This solution was filtered and the filtrate left to sit in a sealed vial. Very small amounts of **5a** deposited as orange blocks. Then **5b** crystallised as yellow blocks while **5c** crystallised as thin red needles and these were separated by eye. M_w 1547.36 (**5a** and **5c**), 1629.46 (**5b**); Yield 2 mg (~8 %); IR: ῡ = 3056 (m), 3026 (m), 2902 (m), 2111 (s), 2074 (s), 1604 (s), 1557 (s), 1526 (s), 1492 (s), 1479 (s), 1450 (s), 1417 (s), 1382 (s), 1359 (s), 1311 (m), 1291 (m), 1256 (s), 1237 (s), 1172 (m), 1154 (m), 1027 (m), 977 (m), 945 (m), 878 (m), 802 (s), 780 (s), 752 (s) cm^{-1}; $C_{84}H_{72}Fe_1N_{18}Se_2$: calcd C 65.20, H 4.69, N 16.29; found C 65.32, H 4.67, N 16.44.

***trans*-[Fe^{II}(DBB)$_2$(NCBH$_3$)$_2$]·2MeCN (6)**

DBB (20 mg, 0.031 mmol) was dissolved in 4 ml methanol. Separately, $NaNCBH_3$ (2 mg, 0.031 mmol), $Fe(ClO_4)_2{\cdot}xH_2O$ (4 mg, 0.015 mmol) and 5 mg ascorbic acid were dissolved in 4 ml acetonitrile. Following one hour of stirring the the methanolic Fe^{II}/$NCBH_3$ solution was added dropwise to the solution of ligand to produce an orange solution. This solution was filtered and the filtrate left to sit in a sealed vial. After two weeks red-orange crystals started to form. M_w 1499.21; Yield ~4 mg (~17 %); IR: ῡ = 3026 (m), 2919 (m), 2324 (s), 2189 (s), 1602 (s), 1569 (s), 1555 (s), 1520 (s), 1494 (s), 1479 (s), 1452 (s), 1420 (s), 1377 (s), 1377 (s), 1357 (s), 1155 (m), 1112 (m), 1076 (m), 976 (m), 943 (m), 873 (m), 776 (s). 757 (s), 696 (s) cm^{-1}; $C_{84}H_{78}Fe_1N_{18}B_2$: calcd C 71.19, H 5.55, N 17.79; found C 70.93, H 5.70, N 18.20.

***trans*-[Fe^{II}(DTBN)$_2$(NCS)$_2$]·2MeOH (7)**
DTBN (20 mg, 0.0497 mmol), NaNCS (4.4 mg, 0.0497 mmol) and $Fe(ClO_4)_2{\cdot}xH_2O$ (6.3 mg, 0.0248 mmol) were dissolved in 5 ml MeOH and stirred with light heating for 30 mins. After this time, the solution was filtered and filtrate left to slowly evaporate. Small yellow needle shaped crystals formed after two weeks. M_w 1037.73; Yield 8 mg (31 %); IR: $\tilde{\nu}$ = 3461 (br), 3104 (s), 3061 (s), 2233 (s), 2056 (s), 1602 (s), 1578 (s), 1556 (s), 1530 (s), 1498 (s), 1465 (s), 1433 (s), 1361 (s), 1317 (s), 1304 (s), 1279 (s), 1232 (s), 1183 (s), 1165 (s), 1121 (s), 1018 (m), 984 (s), 971 (m), 862 (m), 797 (m), 774 (m), 666 (m), 639 (m) cm^{-1}; $C_{42}H_{24}Cl_2Fe_1N_{16}O_6S_2$: calcd C 51.71, H 2.48, N 22.97; found C 51.41, H 2.38, N 22.78.

Supporting Information. (see footnote on the first page of this article). Figures S1 to S9 show crystal structure details and intermolecular contacts of complexes **1**, **3**, **4**, **5a**, **5b**, **5c** and **7**. Table S1 gives selected bond distances and angles of all complexes while Table S2 includes octahedral distortion parameters.

Acknowledgments

This work was supported by an ARC Discovery Grant to KSM. Part of the crystallographic work was performed at the Australian Synchrotron MX1 and MX2 beamlines and we thank the staff for their help. The authors thank Associate Professor David Harding, University of Walailak, Thailand, for valuable discussions on intermolecular effects, spin crossover and cooperativity.

Keywords: Spin Crossover / LIESST / Iron(II) / Magnetic Properties / Dipyridylamine/Intermolecular interactions

[1]. (a). M. A. Halcrow, *Spin Crossover Materials. Properties and Applications*, ed., Wiley, London, **2013**; (b). Special Issue: Spin-Crossover Complexes (Cluster Issue), *Eur. J. Inorg. Chem*., **2013**, *5-6*; (c). P. Gütlich, H. A. Goodwin, eds. Spin crossover in Transition Metal Compounds I-III, *Top. Curr. Chem.,* **2004**, *232-235*, Springer Verlag, Berlin/Heidelberg, Germany.

[2]. (a). J. A. Real, A. B. Gaspar, C. M. Muñoz, *Dalton Trans*., **2005**, *12*, 2062; (b). J. Krober, E. Codjovi, O. Kahn, F. Groliere, C. Jay, *J. Am. Chem. Soc*., **1993**, *115*, 9810; (c). J.-F. Létard, P. Guionneau, E. Codjovi, O. Lavastre, G. Bravic, D. Chasseau, O. Kahn, *J. Am. Chem. Soc*., **1997**, *119*, 10861; (d). S. Hayami, Z. Gu, H. Yoshiki, A. Fujishima, O. Sato, *J. Am. Chem. Soc*., **2001**, *123*, 11644.

[3]. (a). F. J. Muñoz-Lara, Z. Arcis-Castillo, C. M. Muñoz, A. J. Rodriguez-Velamazan, A. B. Gaspar, J. A. Real, *Inorg. Chem.,* **2012**, *51*, 11126; (b). A. Bhattacharjee, M. Roy, V. Ksenofontov, J. A. Kitchen, S. Brooker, P. Gütlich, *Eur. J. Inorg. Chem*., **2013**, *5-6*, 843.

[4]. S. Decurtins, P. Gütlich, C. P. Köhler, H Spiering, A. Hauser, *Chem. Phys. Lett.* **1984**, *105*, 1.

[5]. (a).T. M. Ross, B. Moubaraki, S. M. Neville, S. R. Batten, K. S. Murray, *Dalton Trans.*, **2012**, *41*, 1512; (b). T. M. Ross, B. Moubaraki, S. R. Batten, K. S. Murray, *Dalton Trans*., **2012**, *41*, 2571; (c). T. M. Ross, B. Moubaraki, K. S. Wallwork, S. R. Batten, K. S. Murray, *Dalton Trans*., **2011**, *40*, 10147; (d). Tamsyn M. Ross, Ph.D. Thesis, Monash University, 2010.

[6]. (a). N. Wannarit, O. Roubeau, S. Youngme, P. Gamez, *Eur. J. Inorg. Chem*., **2013**, 730; (b). N. Wannarit, O. Roubeau, S. Youngme, S. J. Teat, P Gamez, *Dalton Trans*., **2013**, *42*, 7120; (c). N. Nassirinia, S. Amani, S. J. Teat, O. Roubeau, P. Gamez, *Chem. Commun*., **2014**, *50*, 1003.

[7]. (a). H. S. Scott, T. M. Ross, S. R. Batten, I. A. Gass, B. Moubaraki, S. M. Neville, K. S. Murray, *Aust. J. Chem*., **2012**, *65*, 874; (b). H. S. Scott, T. M. Ross, N. F. Chilton, I. A. Gass, B. Moubaraki, G. Chastanet, N. Paradis, J.-F. Létard, K. R. Vignesh, G. Rajaraman, S. R. Batten, K. S. Murray, *Dalton Trans*., **2013**, *42*, 16494.

[8]. (a). G. Dupouy, M. Marchivie, S. Triki, J. Sala-Pala, J.-Y. Salaun, C. J. Gomez-Garćıa, P. Guionneau, *Inorg. Chem.,* **2008**, *47*, 8921; (b). S. Hayami, K. Hiki, T. Kawahara, Y. Maeda, D. Urakami, K. Inoue, M. Ohama, S. Kawata. O. Sato, *Chem. Eur. J*., **2009**, *15*, 3497; (c). K. S. Murray, C. J. Kepert, *Top. Curr. Chem.,* **2004**, *233*, 195.

[9]. P. Guionneau, M. Marchivie, G. Bravic, J.-F. Letard, D. Chasseau, *Top. Curr. Chem.*, **2004**, *234*, 97.

[10]. M. Marchivie, P. Guionneau, J.-F. Letard, D. Chasseau, *ActaCrystallogr., Sect. B*, **2005**, *61*, 25.
.

[11]. J.-F. Létard, L. Capes, G. Chastanet, N. Moliner, S. Létard, J.A. Real, O. Kahn, *Chem. Phys. Lett.,* **1999**, *313*, 115.

[12]. (a). J.-F. Létard, P. Guionneau, O. Nguyen, J. S. Costa, S. Marcén, G. Chastanet, M. Marchivie, L. Capes, *Chem. Eur. J.,* **2005**, *11*, 4582 ; (b). J.-F. Létard, *J. Mater. Chem.,* **2006**, *16*, 2550; (c) J.-F. Létard, G. Chastanet, P. Guionneau, C. Desplanches, (Ed. M. A. Halcrow), John Wiley & Sons, Chichester, UK, **2013**, 475.

[13]. X. Feng, C. Mathonière, Ie-R. Jeon, M. Rouzières, A. Ozarowski, M. L. Aubrey, M. I. Gonzalez, R.Clérac, J. R. Long, *J. Am. Chem. Soc.,* **2013**, *135*, 15880.

[14]. W. Phonsri, D.J. Harding, P. Harding, K. S. Murray,B. Moubaraki, I. A. Gass, J. D. Cashion, G. N. L. Jameson, H. Adams, *Dalton Trans.* **2014**, *43*, 17509.

[15]. W. Phonsri, PhD Thesis, University of Walailak, Thailand, 2014.

[16]. S. Hayami, K. Hiki, T. Kawahara, Y. Maeda, D. Urakami, K. Inoue, M. Ohama, S. Kawata and O. Sato, *Chem. – Eur. J.,* **2009**, *15*, 3497.

[17]. G. M. Sheldrick, SADABS, Program for area detector adsorption correction, Institute for Inorganic Chemistry, University of Göttingen, Germany, **1996**.

[18]. T. M. McPhillips, S. E. McPhillips, H. J. Chiu, A. E. Cohen, A. M. Deacon, P. J. Ellis, E. Garman, A. Gonzalez, N. K. Sauter, R. P. Phizackerley, S. M. Soltis, P. Kuhn, Blu-Ice and the Distributed Control System: software for data acquisition and instrument control at macromolecular crystallography beamlines, *J. Synchrotron Radiat.*, **2002**, *9*, 401.

[19]. W. Kabsch, *J. Appl. Crystallogr*., **1993**, *26*, 795.

[20]. CrysAlisPro, Oxford Diffraction Ltd.,Version 1.171.35.15 (release 03-08-2011 CrysAlis171 .NET).

[21]. (a). G. M. Sheldrick, SHELXL-97, Program for refinement of crystal structures, University of Göttingen, Germany, 1997; (b). A. L. Spek, *ActaCrystallogr., Sect. A,* **1990**, *46*, C34.

[a] Dr. H. S. Scott, Dr. T. M. Ross, Dr. W. Phonsri, Dr. B. Moubaraki, Prof. S. R. Batten, Prof. K. S. Murray*
School of Chemistry
Building 23
Monash University
Clayton
Victoria, 3800
Australia
E-mail: keith.murray@monash.edu
Web page:http://monash.edu/science/about/schools/chemistry/staff/murray.html

[b] Dr. G. Chastanet, Prof. J.-F. Létard
CNRS
Université de Bordeaux
ICMCB
87 avenue du Cr. A. Schweitzer
33608, Pessac
France

[c] Prof. S. R. Batten
Department of Chemistry
Faculty of Science
King Abdulaziz University
Jeddah
Saudi Arabia

Supporting information for this article is given via a link at the end of the document.((Please delete this text if not appropriate))

Entry for the Table of Contents (Please choose one layout)

Layout 1:

FULL PAPER

Text for Table of Contents

New mononuclear spin crossover compounds of type *trans*-$[Fe^{II}(NCX)_2(L)_2]$•Solvent have been synthesised and structurally characterised. The L ligands are chelated to Fe by dipyridylamine groups and have aromatic substituents on the central triazine ring that influence cooperativity effects monitored by magnetic and LIESST measurements.

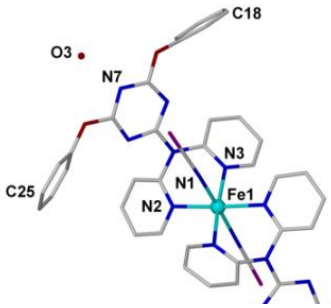

Hayley S. Scott,[a] Tamsyn M. Ross,[a] Wasinee Phonsri,[a] Boujemaa Moubaraki,[a] Guillaume Chastanet,[b] Jean-François Létard,[b] Stuart. R. Batten,[a] and Keith S. Murray*[a]

Page No. – Page No.

Discrete Fe(II) spin crossover complexes of 2,2'-dipyridylamino-substituted s-triazine ligands with phenoxo, cyanophenoxo and dibenzylamino functionalities